Correcting Multibeam Echosounder Bathymetric Measurements for Errors Induced by Inaccurate Water Column Sound Speeds

Haji Mohammadloo, Tannaz; Snellen, Mirjam; Renoud, Weston; Beaudoin, Jonathan; Simons, Dick

DOI
10.1109/ACCESS.2019.2936170

Publication date
2019

Document Version
Final published version

Published in
IEEE Access

IEEE Access
Multidisciplinary | Rapid Review | Open Access Journal

Received June 28, 2019, accepted August 7, 2019, date of publication August 19, 2019, date of current version September 11, 2019.

Digital Object Identifier 10.1109/ACCESS.2019.2936170

Correcting Multibeam Echosounder Bathymetric Measurements for Errors Induced by Inaccurate Water Column Sound Speeds

TANNAZ H. MOHAMMADLOO[1], MIRJAM SNELLEN[1], WESTON RENOUD[2], JONATHAN BEAUDOIN[3], AND D. G. SIMONS[1]

[1]Acoustics Group, Delft University of Technology, 2629 HS Delft, The Netherlands
[2]QPS B.V., Netherlands Office, 3707 NH Zeist, The Netherlands
[3]QPS B.V., Canadian Office, Fredericton, NB E3B 1P9, Canada

Corresponding author: Tannaz H. Mohammadloo (t.hajimohammadloo@tudelft.nl)

ABSTRACT In this contribution a method for correcting bathymetric measurements affected by inaccurate water column sound speed profiles (SSPs) is presented. The method exploits the redundancy in the multibeam echosounder measurements obtained from the overlap of adjacent swaths by minimizing the difference between depths along overlapping swaths. Two optimization methods are used, i.e., Differential Evolution (DE) and Gauss-Newton (GN). While DE inverts for the sound speed by minimizing the depth variation, GN inverts for both bathymetry and sound speed by minimizing the squared sum of the differences between the modeled and measured travel times. The inversion method assumes a constant SSP in the water column. Applying the method to a salt wedge survey area with large variations in the water column sound speed indicates a good agreement between the original depth measurements and those derived after the inversion with the mean and standard deviation of the depth differences equaling 0.009m and 0.024m, respectively. This indicates that even with a simple parametrization of the sound speed in the water column, the correct bathymetry can be derived from the inversion. The SSP inversion method is also applied to an area with existing refraction artefacts. It corrects the bathymetry and reduces the mean and standard deviation of the depth standard deviation by a factor of around 2.75 compared to the case where the measured SSPs were used. Furthermore, the SSP inversion method neither manipulates the existing morphology nor introduces artificial bathymetric features in the areas where such refraction artefacts are not present. Considering constant SSPs, both DE and GN give almost identical results with GN being faster. However, GN is less flexible with regards to varying sound speed parameterizations.

INDEX TERMS Differential evolution, Gauss-Newton, multibeam echosounder depth measurements, optimization methods, refraction induced artefacts.

I. INTRODUCTION

Multibeam echosounder (MBES) systems are widely used for conducting bathymetric surveys. They allow for efficient surveying of large areas and offer the possibility of complete bottom coverage. The MBES sends out an acoustic pulse along a wide swath perpendicular to the sailing direction. Beamsteering at reception allows for determining the travel time of the signals for a set of predefined beam angles [1]. For each ping, water depths along the swath are derived from the combination of travel times and beam angles, provided that the local Sound Speed Profile (SSP) in the water column is known [2].

In principle, towed systems, such as a Moving Velocity Profiler (MVP) or an underway Conductivity, Temperature, Pressure (CTD) sensor [3], [4] can be used to acquire SSP measurements. However, they are not widely applied due to the risk of fouling or grounding of the towed instrumentation with each cast. Instead, non-towed systems are often used where the speed of sound in the water is measured by lowering a velocimeter or CTD sensor in the water as deep as possible. To perform such a measurement, the vessel needs to remain stationary. This makes the acquisition of SSP measurement a time-consuming process, and is thus impractical

The associate editor coordinating the review of this article and approving it for publication was Marko Beko.

to obtain these measurements at high rates. While infrequent acquisition of the SSP is expected to play a minor role in environments with little variations of sound speeds (both temporally and spatially), it is expected to have large effects on the depth measurements in highly dynamic environments where the varying presence of salt and fresh water results in large variations in the SSP leading to systematic errors in the estimate for depth and position of the soundings.

The effect of using erroneous sound speeds on derived bathymetry has been discussed by numerous scholars. References [5] and [6] examined the effect for a flat transducer (zero roll and mounting angle). References [5] and [7] showed that for a MBES with zero mounting angle and roll, the varying error terms induced by the erroneous sound speed profile cancel out each other at 45° beam angle, and thus regardless of the SSP, the measured depth is always equal to the true depth for this angle. Reference [8] studied the impact of erroneous SSPs for a tilted array and concluded that the angular error depends on the sign and magnitude of roll and is thus related to the motion time series. References [9] and [10] designed a numerical simulation tool to assess the impact of water column variability on sounding uncertainty without any requirement for soundings. Reference [11] created a map of the depth uncertainty using raytracing based on the spatial variability of two popular oceanographic data sources. Such a tool allows for the identification of areas of high water column variability and the evaluation of seasonal variations of errors due to imperfect knowledge of the environment.

Approaches to compensate for a lack of sound speed information have been studied and range from reducing the need for sound speed information to gathering additional sound speed information. Reference [12] proposed an equivalent yet, simplified representation for the SSP which can significantly increase the speed of the ray tracing algorithm. Determination of the minimum sampling rate for SSPs was done by [13].

One can also deal with a lack of SSP information by filling the gaps between the succeeding measurements. Reference [14] developed a model for generating mean SSPs for any location in the world using global oceanic databases. However, the SSP derived can deviate from that present at the time of the measurements, particularly in small-scale highly dynamic environments. A number of approaches have been proposed using model predictions of the prevailing water column SSP in such circumstances. Such a method is incorporated in the Adaptive Bathymetric Estimation (ABE) method, introduced by [15] and extended by the same authors in [16], using estimates of the SSP based on a model for the bathymetry using the Extended Kalman Filter. Reference [17] used an oceanographic model that incorporates surface and internal waves and has a high spatio-temporal resolution to generate the SSP for refraction correction. When deriving depth estimates from the measured travel times, however, such a database might not be always available.

Effort has been put forward to correct the MBES derived depths affected by refraction artefacts. Reference [18] presented a refraction correction algorithm in a post-processing context. The method takes into account the nadir data of either two neighbor parallel sailed tracks or crossing tracks. It then searches for refraction coefficients of a two-layer SSP that brings the outer parts of the sailed tracks as close as possible to the seafloor observed at nadir. The method thus assumes that the shape of the swath corrected for refraction artefacts is aligned with the nadir depths of other surrounding lines. However, this assumption can be violated if a large angular coverage (large swaths) is considered resulting in the possibility of the existence of real bathymetric features at the outer parts of the swaths which do not exist at nadir. Reference [19] adopted a relatively similar approach by using the measured depth and considering this as the true depth for the outer parts of the swath. This true depth, in combination with other parameters such as beam angle and two-way travel time, was used to invert for the constant gradient SSP. Reference [20] proposed an inversion method using Empirical Orthogonal Functions.

It is standard practice to carry out MBES surveys with at least a small overlap between adjacent swaths (derived from adjacent sailed tracks). The time between measuring two overlapping swaths typically amounts to maximum several hours, but this can vary greatly depending on water depth and survey type (e.g. route survey, charting). Since generally sediment transport does not occur in a period less than several days or weeks, i.e. bottom features such as mega ripples and sand waves are not expected to vary within this relatively short period, the bottom can be assumed to be stable over the course of the survey. Consequently, the depths as determined from the measured travel times along the two overlapping swaths should be the same at equal points on the seafloor. However, for environments with strong variations in the water column SSP, sometimes significant differences are found. For modern well-calibrated MBES systems, these differences are in general due to the use of an erroneous sound speed profile stemming from a lack of and/or incorrect sound speed information.

In this contribution, we propose a method for estimating the sound speed and depth that fully employs the redundancy of the overlapping MBES swaths. The importance of the present contribution can be thus assessed from two perspectives. Firstly, it provides one with the possibility to correct the bathymetric measurement in case of having erroneous or insufficient knowledge about SSPs. Secondly, it reduces the need to acquire frequent SSP measurements, which is a time-consuming process, and thus, survey efficiency can be increased.

Assuming negligible depth variations due to seafloor dynamics and minimizing the contribution of systematic error sources affecting the depth measurements, sound speeds are estimated by minimizing the difference between the water depths along the overlapping parts. Minimization of the water depth variations along the overlapping swaths (optimizing the sound speeds) is carried out using Differential Evolution (DE), [21], and Gauss-Newton (GN), [22]. The former

can be classified as a meta-heuristic method making few or no assumptions about the problem being optimized and can search very large spaces. DE was found to be an efficient global optimization method to solve inversion problems in underwater acoustics and is generally more efficient than the original Genetic Algorithm (GA) when searching for the global optimum of a real geo-acoustic inversion problem. DE is used for multi-dimensional real-valued functions and does not require the calculation of the gradient of the problem being optimized. However, a large number of forward calculations are required to obtain the optimal solution. A faster alternative is thus to use a gradient-based optimization method, such as GN, with the risk of converging to a local minimum. GN is used to solve non-linear least squares problems and is a modification of the Newton's method with the advantage of not requiring the second derivatives of the optimization problem.

Within the present contribution, a simple description of the water column sound speed, i.e., constant sound speed, is assumed. However, data taken in a complex environment with varying water column sound speeds with depth (salt wedge estuary) is used and the performance of the method with the assumption of constant SSP is assessed. As a next step, the proposed method is applied to an area with refraction artefacts. A comparison is also made between the two optimization approaches, DE and GN.

This paper is organized as follows. In Section II the method for reducing the SSP induced bathymetric errors is introduced. Section III gives the description of the MBES data sets used. The data were acquired during a routine bathymetric survey, i.e., they reflect standard practice. In Section IV the results of applying the inversion algorithm are presented, followed by the conclusion drawn in Section V.

II. CORRECTING SOUND SPEED INDUCED BATHYMETRIC ERRORS

A. THE ROLE OF WATER COLUMN SOUND SPEEDS IN MBES BATHYMETRIC MEASUREMENTS

Insufficient knowledge about the water column sound speed hampers correct determination of water depths in two ways as addressed in the following, and results in a concave (referred to as smiley or curved upward) or convex (referred to as frowny or curved downward) seabed surface distortion. Here, a simple situation is considered with a constant sound speed over the entire water column. However, the approach presented is not limited to such assumption.

1) EFFECT ON SOUND PROPAGATION

Sound is impinging on the MBES at angle θ with respect to the normal of the MBES, see Fig. 1. One can determine the location on the seafloor from which the sound is scattered to the transducer using θ, MBES mounting angles and SSPs. An error in the SSP will thus result in an erroneous estimate of this location.

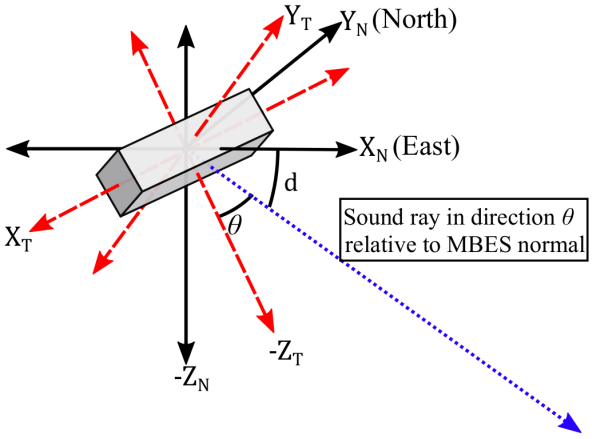

FIGURE 1. MBES measurement configuration schematic. X_T, Y_T and Z_T denote the transducer frame. X_N, Y_N, Z_N indicate the navigation frame. θ and d are the beam angles of the sound ray relative to the MBES normal and navigation horizontal plane respectively.

2) EFFECT ON BEAMSTEERING

The MBES transmits a sound pulse over a wide range of angles perpendicular to the sailing direction. Beamsteering at reception is applied for discriminating between the directions from which the sound impinges at the MBES after backscattering from the seafloor. For a linear array made of independent receiving elements located at equal distances, beamsteering in direction θ for a receiving element i comes down to applying a time delay τ_i of

$$\tau_i = \frac{(i-1)L\sin\theta}{v}, \tag{1}$$

with L being the distance between the individual receiving elements of the receiver array. Employing an erroneous sound speed for the beamsteering, referred to as v_m, instead of the true one, v, thus introduces errors in the time delays applied. Consequently, the actual steering angle, θ_m, differs from the direction aimed for, θ.

B. THE OPTIMIZATION METHODS CONSIDERED

Fig. 2(a) shows the MBES survey geometry, consisting of a number of tracks that have been sailed parallel to each other, such that the MBES swaths from the adjacent sailed tracks have a certain overlap with each other. The MBES measurements consist of measured two-way travel times for all beams. Fig. 2(b) shows the depths along a cross-section for a situation where the SSPs used are erroneous, resulting in the depth differences at the overlapping parts. Assuming calibrated mounting offsets and accurate (high quality) tide observations, heave, and draft or 3-dimensional positioning with Global Navigation Satellite System (GNSS), the remaining difference in the water depths at the overlapping parts are mostly attributable to the use of incorrect SSPs (this issue will be elaborated later on) allowing for its estimation through optimization of an objective function based on the depth differences along overlapping parts of the swaths.

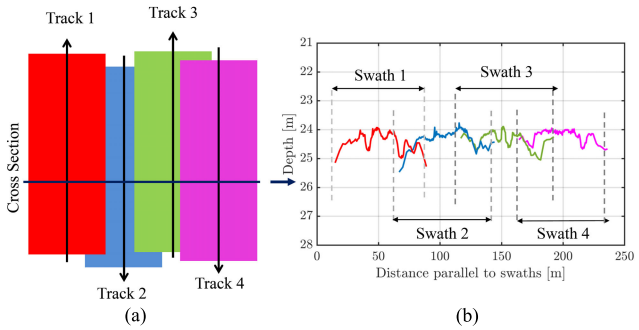

FIGURE 2. (a) Schematic of survey configuration. The arrows indicate the sailing direction, (b) Example of differences in estimated bathymetry due to insufficient information about the water column sound speed for the cross section containing depth measurements from four sailed tracks.

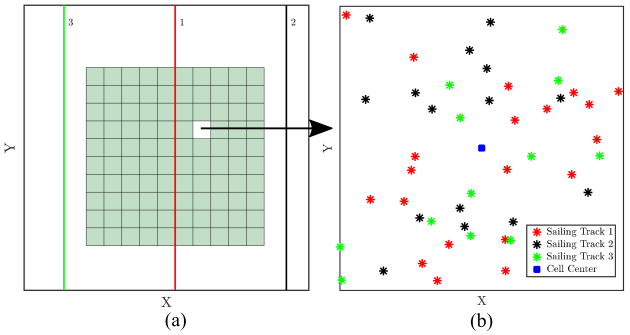

FIGURE 3. (a) Schematic overview of the grid considered for a segment of the survey area and (b) a cell in the grid which contains the depth measurements from three adjacent sailing tracks.

Hereto, the optimized sound speeds are derived by minimizing the depth differences along these overlapping parts. Since both the time and position of the MBES measurement differ for each of these swaths, their sound speeds are expected to be different for them as well. This means that for a part of the survey area where the depth measurements from N overlapping swaths exist, the search should be carried out for unknown parameters needed for the description of N SSPs.

1) DIFFERENTIAL EVOLUTION

For the first approach use is made of the Differential Evolution (DE), which is a global optimization method and is a variant of the well-known Genetic Algorithm (GN), and the following steps are taken. For a number of consecutive pings in a given sailed track, the part of the seafloor where the depth measurements from this track and its adjacent tracks overlap is considered and is referred to as a 'segment' for the remainder of this work. For quantifying the agreement in water depths at the overlapping parts, a grid aligned to the mean heading of the pings in the track under consideration is defined, i.e., the X and Y axis of the grid are assumed to be perpendicular and parallel to the heading direction, respectively, see Fig. 3(a). To implement the DE method, the energy (objective) function is defined as

$$E(\mathbf{x}) = \sum_{c=1}^{C} \sqrt{\frac{\sum_{n=1}^{N} \sum_{k=1}^{K_{c,n}} (z_{c,n,k}(\mathbf{x}) - \bar{z}_c(\mathbf{x}))^2}{\sum_{n=1}^{N} K_{c,n}}} \qquad (2)$$

where C is the total number of grid cells in the segment considered (as an example 100 cells in Fig. 3(a)) and $K_{c,n}$ is the total number of measurements of a given sailed track (n) located within a given cell (c). $\mathbf{x}$ contains the parameters needed for the description of the N SSPs for the segment under consideration. For the current contribution, constant sound speed profiles are assumed. This means that $\mathbf{x}$ contains N unknown sound speeds. For the example shown in Fig. 3, we have thus $N = 3$. $z_{c,n,k}$ is a single depth (k) of a given track located in a given cell and $\bar{z}_c$ is the weighted mean of $z_{c,n,k}$ with the weight function being the inverse cubed horizontal distance between the location of the measurements and the cell center. Fig. 3(b) illustrates the situation for one cell within the grid which contains the depth measurements from three sailed tracks (shown with varying colors). $K_{c,1}$, $K_{c,2}$ and $K_{c,3}$ indicate the number of depth measurements from sailed tracks 1, 2 and 3, respectively.

When an update value for the n^{th} track sound speed is available, the beam vector, see Fig. 1, has to be re-pointed, and consequently $z_{c,n,k}$ is recalculated. Traditionally, re-pointing a beam to account for an update of the sound speed at the transducer is done by correcting the raw steering angles θ reported by the transducer followed by recalculating the beam launch angle, d in Fig. 1, see [23], [24]. However, in this contribution the refraction correction is applied to the launch angle, without having to recalculate θ. This leads to an increase in the processing speed. The energy function, $E(\mathbf{x})$, calculated for each segment, is minimum when the depth variations for each cell are minimized. This implies that the depths corresponding to the measurements from adjacent sailed tracks have become closer to each other. Consequently, minimization of the energy function gives the sound speeds which provide the maximum agreement between water depths for the segment considered. In order to locate the minimum of (2), use is made of DE [21]. Details on this algorithm are provided by [25]. The lower and upper bounds for the unknown sound speeds are assumed 1400m/s and 1600m/s respectively. The performance of global optimization methods, i.e., their success in locating the global optimum in an efficient way, is dependent on a number of so-called setting parameters. For the DE, these are

- Population size q
- Multiplication Factor F
- Crossover Probability p_c
- Number of Generations N_G

These setting parameters have to be set beforehand to maximize the probability to locate the global optimum. In this work the best values for these parameters while preserving the computational efficiency were found to be $q = 16$, $F = 0.6$, $p_c = 0.55$ and $N_G = 10N$.

2) GAUSS NEWTON

The method presented above describes an approach to reduce SSP induced errors by searching for SSPs maximizing the

agreement in water depths along the overlapping parts covered by adjacent sailed tracks. In principle, DE allows for an arbitrary SSP parameterization. However, it requires a significant number of forward calculations.

For reducing the computational effort, instead of DE, the Gauss-Newton (GN) method can be used for the optimization. For the DE optimization, the parameters searched for are the SSPs per sailed track located within the segment under consideration. For the GN, a different approach is taken, where both the SSPs and water depths are considered unknown and the aim is to minimize the function

$$G = \sum_{c=1}^{C} \sum_{n=1}^{N} \sum_{k=1}^{K_{c,n}} (t_{c,n,k} - T_{c,n,k})^2 \tag{3}$$

where $t_{c,n,k}$ and $T_{c,n,k}$ are the modeled and measured one-way travel time (OWTT) of the k^{th} depth measurement from a given sailed track in the given cell (c), respectively. The model for calculating $t_{c,n,k}$ accounts for the effects of the sound speed on the beamsteering and propagation through the water column. Assuming each cell in the overlapping part is a horizontal plane with the normal vector of $[0, 0, 1]$, the intersection of a vector containing the MBES position at the time of transmission and passing through a given depth measurement (k) in a given track with the plane can be computed, see Fig. 4. The equation of the plane with the above normal vector containing the center of the given cell reads as

$$z = z_c \tag{4}$$

where z is the depth of an arbitrary point on the plane and z_c is the depth of a given cell (c). Equation (4) implies that the depth in a cell is constant (it can vary from one cell to another). The vector form of the equation defining a given depth measurement (k) in a given track (n) transmitted from the MBES, i.e., the equation of a line passing through the MBES at the time of transmission of a given beam with

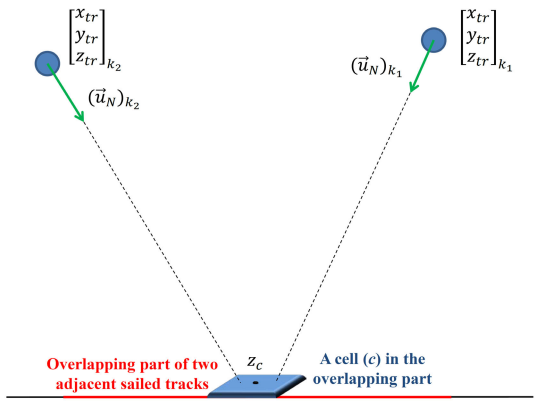

FIGURE 4. Schematic overview of a cell in the overlapping part of the two adjacent sailed tracks (1 and 2) in the navigation frame. The rotations roll, pitch and heading are not shown here for the sake of clarity. Indices k_1 and k_2 indicate two depth measurements from the sailed tracks 1 and 2 respectively.

the directional vector of $\vec{u}_N$ reads as (see the dashed lines in Fig. 4)

$$\begin{bmatrix} x \\ y \\ z \end{bmatrix} = \begin{bmatrix} x_{tr} \\ y_{tr} \\ z_{tr} \end{bmatrix} + \vec{u}_N s \tag{5}$$

where s is a scalar describing an arbitrary point on the line, and $\vec{u}_N$ is given in (A.1). The vector $[x_{tr}, y_{tr}, z_{tr}]^T$ contains the transducer horizontal coordinates and depth in the navigation frame at the time of transmitting the signal corresponding to given depth measurement k in a given track n. To clarify this, take Fig. 4 as an example which illustrates a cell in the overlapping part of the two adjacent sailed tracks (referred to as 1 and 2) containing the depth measurements from both of them. The indices k_1 and k_2 indicate a depth measurement from sailed tracks 1 and 2 with their associated unit vectors in the navigation frame $(\vec{u}_N)_{k_1}$ and $(\vec{u}_N)_{k_2}$, respectively. For the intersection of (5) with the seafloor, $x = x_{c,n,k}$, $y = y_{c,n,k}$ and $z = z_{c,n,k}$ is considered, with $x_{c,n,k}$ and $y_{c,n,k}$ being the horizontal position of a depth measurement from a given sailed track located in a given cell. The intersection of this line with the plane is derived by substituting (5) in (4) and solving for s ($s = \frac{(z_{tr} - z_c)}{z_N}$ with $z_N = -\sin d$ being the third component of the beam unit vector in the navigation frame, see (A.1)). Substituting s in (5) and considering the measured depth to the seafloor, the OWTT can be modeled as

$$t_{c,n,k} = \frac{z_{tr_{n,k}} - z_c}{v_n \sin(d'_{c,n,k}(v_n))} \tag{6}$$

where v_n is the sound speed corresponding to the n^{th} sailed track. $d'_{c,n,k}(v_n)$ is the launch angle (see Fig. 1) which is a non-linear function of the sound speed and the symbol $'$ indicates that it has been recalculated using the updated sound speed. As mentioned, the unknowns to be determined are the sound speeds of the sailed tracks located in the segment under consideration and the depths of the cells' center, i.e., v_n and z_c. It is seen from (6) that there exists a nonlinear relation between the unknowns and modeled travel times. By linearizing (6) one gets

$$E\{\mathbf{y}\} = A(\mathbf{x}); D\{\mathbf{y}\} = \sigma^2 \mathbf{I} \tag{7}$$

where $\mathbf{x} = [z_1, z_2, \ldots, z_C, v_1, v_2, \ldots, v_N]^T$ is a vector of length $C + N$ containing the unknowns. $\mathbf{y}$ indicates vector of the length $\sum_{n=1}^{N} K_{c,n}$ containing the measured-minus-modeled OWTT (residual vector). $\sigma^2\mathbf{I}$ is the covariance matrix of $\mathbf{y}$ with σ^2 the variance of the data and $\mathbf{I}$ an identity matrix. $\boldsymbol{A}$ is the linearized design matrix of the size $\sum_{n=1}^{N} K_{c,n} \times (C+N)$. Its columns indicate the partial derivatives of (6) with respect to the unknown parameters ($\mathbf{x}$) as

$$\begin{aligned} \frac{\partial t_{c,n,k}}{\partial z_c} &= \frac{-1}{v_n \sin(d'_{c,n,k}(v_n))} \\ \frac{\partial t_{c,n,k}}{\partial v_n} &= \frac{(z_c - z_{tr_{n,k}})\left(\frac{\partial d'_{c,n,k}(v_n)}{\partial v_n} \cot(d'_{c,n,k}(v_n)) + \frac{1}{v_n}\right)}{v_n \sin(d'_{c,n,k}(v_n))} \end{aligned} \tag{8}$$

Solving for **x** in a least-squares sense conform (3) requires an iterative GN approach, see for example [26].

It should be highlighted that although the apparent formulation of the objective functions used in GN and DE is different, they both aim at minimizing the depth variations located at the overlapping areas of adjacent sailed tracks. For the DE, this is done by directly minimizing the difference between depth measurements. For the GN, sound speeds are sought for that optimally (in terms of difference between measured and modeled OWTT) allow for representing the water depths at each cell by a constant value. This indicates that the above two methods are conceptually equivalent.

III. DESCRIPTION OF THE DATA SETS

For the assessment of the performance of the SSP inversion method, two data sets are used. The first one is acquired by Rijkswaterstaat in the Nieuwe Waterweg, The Netherlands, which is a ship canal from het Scheur (a branch of the Rhine-Meuse-Scheldt delta) west of the town of Maassluis to the North Sea at Hook of Holland. The data was acquired on the 19th of January 2010 using a Reson 8125 MBES and covers an area of 270000m^2 consisting of 19 sailed tracks with water depths varying from 3.5m to 26m, see Fig. 5. The data set is acquired within the time span of 2h and 45min. Fig. 6 illustrates the water level with respect to NAP (Normaal Amsterdams Peil) vertical datum for the Maeslantkering sea side tide station (closest station to the survey area). During this period, the maximum water level variation for this station is around 0.16m. The bottom morphology is not expected to change to a noticeable extent. The survey area is characterized by a sand wave field which is traversing the sill plates of the Maeslantkering storm surge barrier and is considered to be a salt wedge estuary with a strongly stratified water mass in which fast

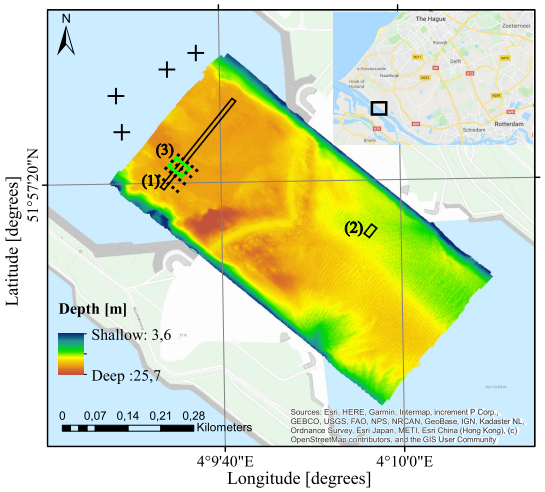

FIGURE 5. Bathymetry and location of the survey area (Nieuwe Waterweg, The Netherlands). The bathymetry map is derived from Qimera post-processing software developed by Quality Positioning Services (QPS) B.V.. The location of the measured SSPs is shown by black crosses. The areas indicated by 1, 2 and 3 and the sailed tracks shown by black dashed lines will be investigated further.

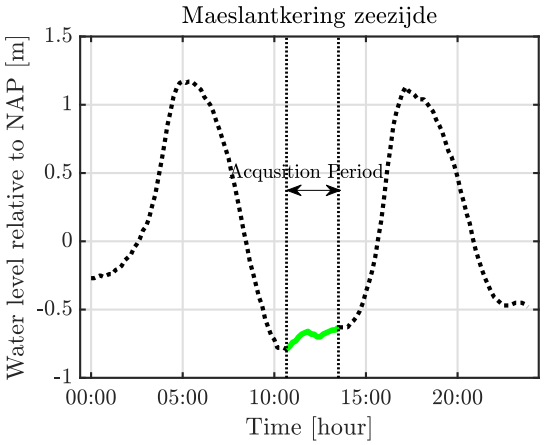

FIGURE 6. Water level with respect to NAP (Normaal Amsterdams Peil) vertical datum for the closest tide station to the data set acquired in Nieuwe Waterweg during the data acquisition period.

flowing surface river water is predominantly fresh and bottom water is predominantly salty with a pronounced pycnocline at the interface between the two layers [9]. The 4 SSPs acquired are shown in Fig. 7. The pycnocline is most apparent between 8m to 12m depth in the SSPs, with sound speeds ranging from approximately 1425m/s to 1450m/s (total range of around 25m/s). The overlapping part between the two adjacent tracks was close to 70%, enabling the assessment of varying the percentage of overlap on the method's performance.

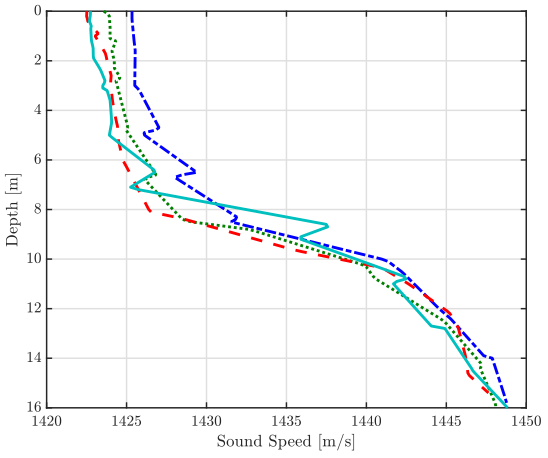

FIGURE 7. The 4 measured SSPs for the survey area (Nieuwe Waterweg).

The second data set considered in this contribution was acquired in the Bedford Basin, Halifax, Nova Scotia, Canada using a multi-frequency R2Sonic 2026 MBES on 2nd of May 2017. This data set was used as one of the primary data sets in R2Sonic's Multi-Spectral Challenge (see [27], [28]). The frequencies used during the data acquisition equal 100kHz, 200kHz and 400kHz. To avoid depth variations due to varying signal penetration with frequency, as observed by [29], the results here are presented considering only the frequency of 200kHz. The data covers an area of around 1840000m^2 and consists of 13 sailed tracks with approximately 50% survey overlap. The depth in the survey

area ranges from 13m to 90m, see Fig. 8. The survey itself is small relative to the entire Bedford Basin. The basin is an estuary situated at the northwest end of Halifax Harbour and is blocked from full ocean circulation by a narrow and shallow sill [30]. This data set was chosen as the refraction problem only exists in the northeast of the survey area. It is thus important to assess whether the application of the SSP inversion method to the complete survey area corrects for the refraction problem only in the areas needed or whether it affects the bathymetry in the remaining parts without refraction induced errors. The latter results in misinterpretation of the bottom morphology. Also, the varying morphology within the survey area makes this data set interesting for assessing the performance of the inversion method.

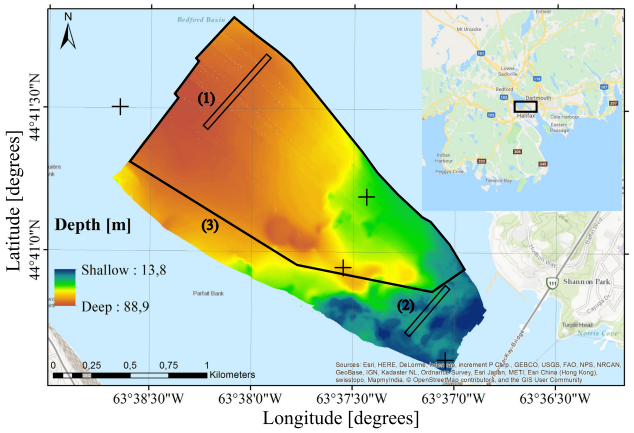

FIGURE 8. Bathymetry and location of the survey area (Bedford Basin, Canada).The bathymetry map is derived from Qimera post-processing software developed by Quality Positioning Services (QPS) B.V.. The location of the SSPs acquired are also shown by black crosses. Areas indicated by 1, 2 and 3 will be investigated further.

IV. RESULTS

A sailed track within the survey area is divided into subsets consisting of 20 consecutive pings. The method considers the part of the seafloor where the depth measurements from these pings in the track under consideration and its adjacent ones overlap. This part is referred to as a segment. A grid is defined for each segment with its X and Y axes perpendicular and parallel to the headings of the pings, respectively. The resolution of the grid in both directions is equal and taken as 10% of the average depth of the measurements located in the segment. This value is chosen as such to ensure the availability of a sufficient number of soundings for calculating the statistics within a cell. Considering that the depth measurements corresponding to the N sailed tracks are located in this segment and assuming constant SSPs, N sound speed are derived (one per sailed track). Afterwards, the next 20 pings are considered and the same approach is applied.

The performance of the inversion method is assessed using two indicators

1) **Difference between the depth measurements.** To assess the inversion method's accuracy, i.e., its unbiasedness, a data set free of refraction artefacts is considered and artificial artefacts are introduced assuming erroneous sound speeds in the water column. The SSP inversion method assuming a constant sound speed is applied to the resulting erroneous depths and the difference between the depths derived after applying the SSP inversion and the original ones is assessed. This also illustrates how the simplified description of the sound speed profile, i.e., considering a constant value, affects the results.
2) **Standard deviation of the depth measurements for each cell of the grid.** If the refraction artefacts do not exist, the standard deviation of the depth measurements in a cell reflects the uncertainty of these measurements (due to the uncertainties inherent to the MBES and those induced by the bottom morphology). However, if the refraction artefacts exist, smiley or frowny features appear and the discrepancies between the depth measurements from the adjacent sailed tracks increase resulting in an increase in the standard deviation. This value can be seen as a measure of the precision of the SSP inversion algorithm.

A. APPLYING DIFFERENTIAL EVOLUTION BASED SSP INVERSION METHOD TO NIEUWE WATERWEG

The high quality data set acquired in the Nieuwe Waterweg is free from refraction artefacts. As seen from Fig. 7, the sound speed in the water column varies with depth and is not constant. We create erroneous SSPs by increasing the measured SSPs by 15m/s for the upper part and decreasing it by 12m/s for the lower part of the water column. Also random Gaussian noise with a standard deviation of 0.2m/s is added to the sound speeds. This value represents the uncertainty in the SSP measurements at different locations (inland waterways and the North Sea). Using the resulting SSPs, ray tracing is carried out and the depths are determined. These depths are thus affected by refraction artefacts. The SSP inversion method assuming a simple representation of the sound speed in the water column is applied to the data affected by the refraction artefacts.

To assess the two surfaces (i.e., original and the one after application of SSP inversion), two small parts of the survey area consisting of around 20 consecutive pings are chosen, see the black rectangles indicated by 1 and 2 in Fig. 5. Area 1 is located in a relatively flat part. Area 2, however, is located in an area with varying morphological features. Shown in Fig. 9(a) and Fig. 10(a) are the original depth measurements derived from raytracing using the measured SSPs. Varying colors indicate different sailed tracks. Using the erroneous SSPs, ray tracing is again carried out and the corresponding depths are calculated. For area 1 (Fig. 9(b)), the resulting depth artefacts are clearly evident (smiley features appear at the overlapping parts). As for area 2 where the bathymetric features exist, see Fig. 10(b), the erroneous SSPs lead to an incorrect interpretation of the bottom morphology.

The DE based SSP inversion method is applied. Fig. 9(c) and Fig. 10(c) show the depths recalculated after

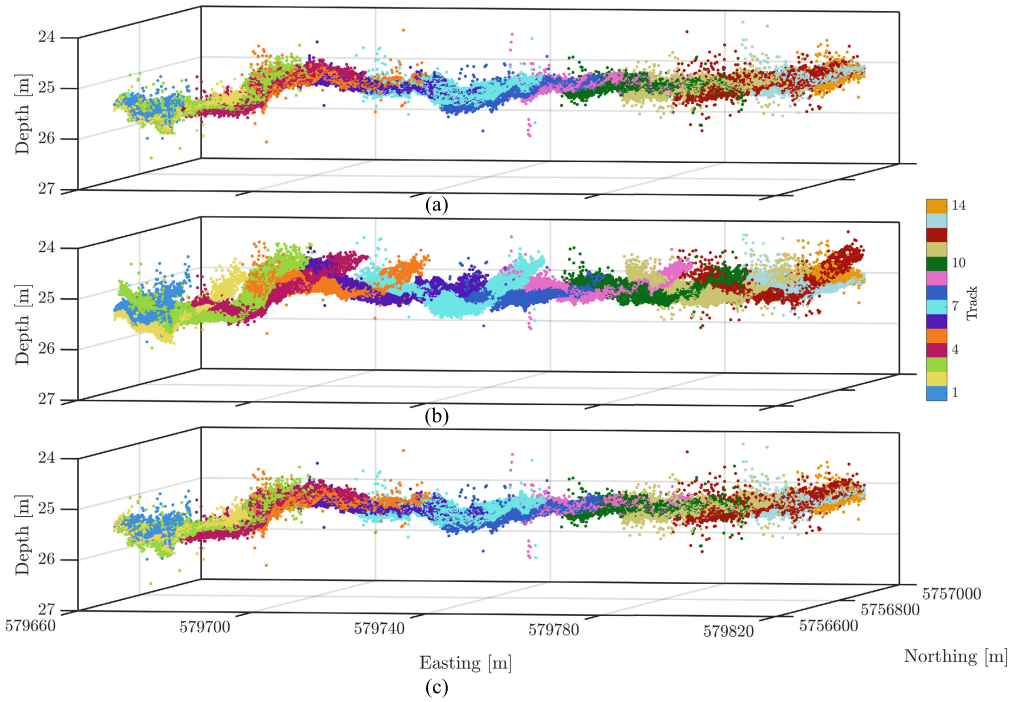

FIGURE 9. Depths within area 1 in Fig. 5 consisting of 20 pings derived from the (a) original SSPs, (b) erroneous SSP and (c) results of the SSP inversion. Varying colors indicate different sailed tracks.

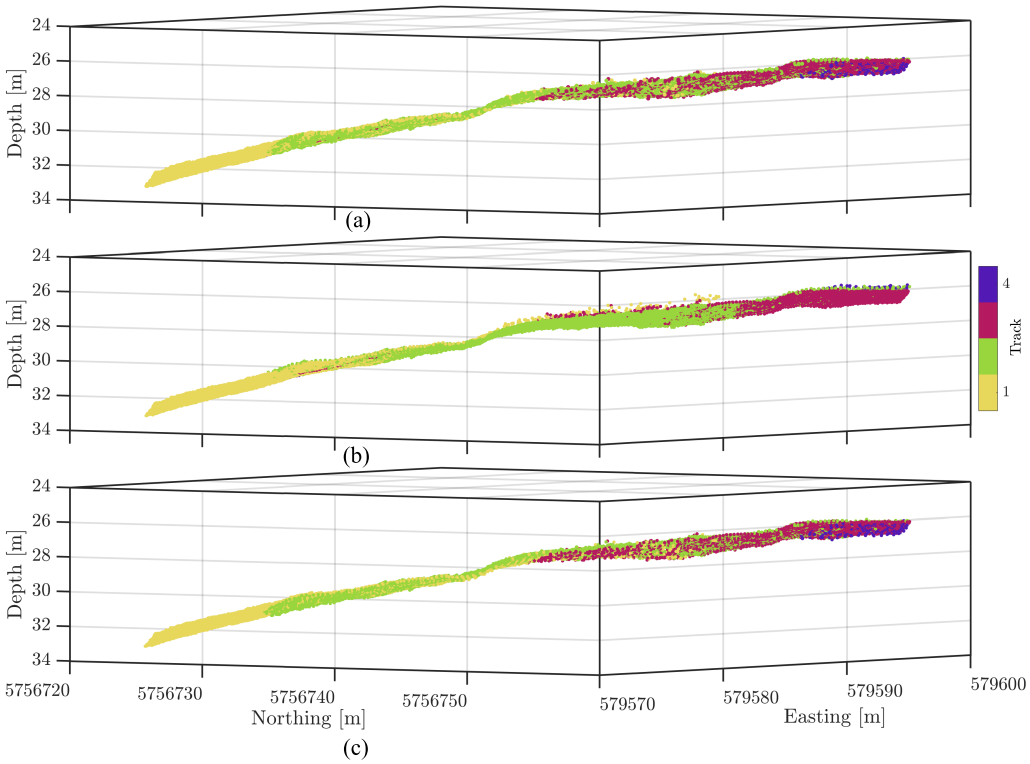

FIGURE 10. Depths within area 2 in Fig. 5 consisting of 20 pings derived from the (a) original SSPs, (b) erroneous SSP and (c) results of the SSP inversion. Varying colors indicate different sailed tracks.

applying the method. A visual comparison between the recalculated depths after the inversion and the original ones, Fig. 9(a) and Fig. 10(a), suggest that although the assumption of constant SSPs does not hold for the data set considered, the inversion method successfully recovers the original surface. For 98% and 90% of the depths in areas 1 and 2 the

difference between the original depths and those derived after SSP inversion is less than 0.023m and 0.035m, respectively. These differences are quite small relative to typical errors associated with MBES systems. This also indicates that at least for these two areas, the application of the SSP inversion method does not affect the bottom morphology such that nonexistent bathymetric features appear or the existing morphology changes. It should be noted that the external disturbances, such as noise from neighbouring vessels, do not affect the detected bottom (they can affect the backscatter strength though), and hence do not affect the SSP inversion method. However, as the method uses the depths at the overlapping parts of the adjacent swaths, pings influenced by potential disturbing sources affecting the depth measurements, such as a school of fish, have to be excluded from the measurements.

As a next step, the difference between the original surface and the one derived after the SSP inversion is assessed for the full area. Shown in Fig. 11 is the histogram of the differences between the original depth measurements and those recalculated after the SSP inversion along with its normal distribution fit (red curve). The mean and standard deviation of the differences ($\triangle$) are 0.009m (vertical solid blue line), $E(\underline{\triangle})$, and 0.024m, $\sigma_{\underline{\triangle}}$, respectively. The differences have to be tested from the statistical point of view to assess whether they are statistically significant. To this end, the null and alternative hypotheses are considered as $H_0 : E(\underline{\triangle}) = 0$ versus $H_1 : E(\underline{\triangle}) \neq 0$. Provided that the number of samples is sufficiently large, based on the central limit theorem one can state that the sample average of these random variables is normally distributed with the mean zero and standard deviation of $\sigma_{\underline{\triangle}}$. A 95% confidence interval for a given sample is obtained by $-1.96\sigma_{\underline{\triangle}} < E(\underline{\triangle}) < 1.96\sigma_{\underline{\triangle}}$, i.e., $-0.048 < 0.009 < 0.048$. Therefore, the differences between the original and inverted depths are not statistically significant.

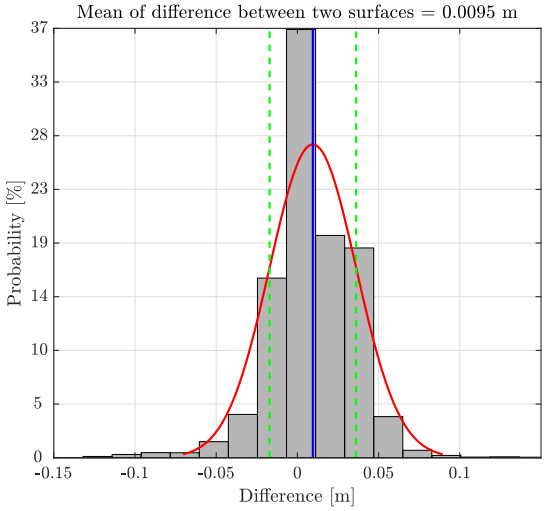

FIGURE 11. Histogram of the difference between original depths and those derived after the SSP inversion and its normal distribution fit (red curve). Shown with the vertical solid blue line is the mean of the differences. The vertical dashed green lines indicate mean ± standard deviation of the differences.

Indicator 2 introduced earlier for the assessment of the SSP inversion method is the standard deviation of the depths after applying the SSP inversion. A grid with a cell size of 0.25m × 0.25m is defined for the full survey area (this cell size can be different from those defined for each segment of the data for applying the SSP inversion method). The standard deviation of the original depth measurements located in each cell is calculated and is assigned to the cell center. For the depths derived assuming erroneous SSPs and those recalculated after the application of the inversion method, the standard deviation is also determined. Shown in Fig. 12(a) is the map of the difference between the standard deviation of the original depths and those based on the erroneous SSPs where a positive value indicates a larger standard deviation of the latter. Using erroneous SSPs results in a noticeable increase in the standard deviation, as seen from the increase (red parts) for the overlapping parts of the sailed tracks. The mean value of the standard deviation over the entire area increases from 0.113m to 0.202m. Fig. 12(b) illustrates the map of the difference between the standard deviation of the original depth measurements and those recalculated after SSP inversion. A visual inspection indicates almost equal depth standard deviations of the two.

The results presented so far are derived from the application of DE. No significant differences were found between the results of applying the DE and GN based SSP inversion methods to this data set.

B. INVESTIGATING THE EFFECT OF OVERLAP PERCENTAGE

As mentioned previously, for the functionality of the SSP inversion method (either DE or GN), overlap between the adjacent swaths is required. An important issue to investigate is the impact of varying overlap percentages. By the overlap percentage we mean the portion of the swath corresponding to one sailed track covered by the swath of the adjacent sailed track. To this end, a small area consisting of 50 pings, indicated as 3 in Fig. 5 and 12 is used where the soundings from 4 tracks (indicated by dashed lines) are located. To define the varying percentages of overlap, 3 different scenarios, depicted as (a), (b) and (c) in Fig. 13 and summarized in Table. 1, are considered. Three sailed tracks indicated as L1, L2 and L3 are shown in this figure. The scenarios are as follows:

- **Scenario a**: The overlap exists between 3 lines, L1, L2 and L3. Fig. 13(a) shows the situation in which these lines and the maximum available swath width are used, resulting in the overlap of 70% between

TABLE 1. Summary of the scenarios (a), (b) and (c) shown in Fig. 13 including the lines used along with the corresponding overlap percentages.

Scenario	Lines used	Overlap percentage (%)
(a)	L1, L2 and L3	70 and 55
(b)	L1 and L2	40 and 35
(c)	L1 and L3	30, 18, 12 and 9

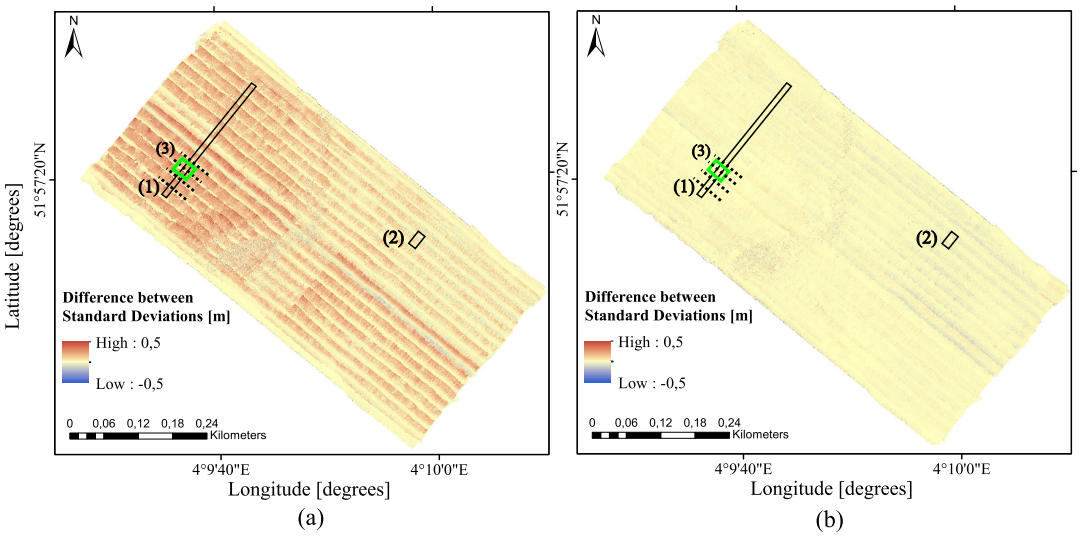

FIGURE 12. Difference between the standard deviation of the original depth measurements of Nieuwe Waterweg and those (a) derived assuming erroneous SSPs, and (b) recalculated after applying the DE inversion method.

TABLE 2. Standard deviation of difference between the original depths and those derived after applying the inversion algorithm for varying percentage of overlap for area 3 (Fig. 5).

Overlap percentage (%)	Depth standard deviation (m)
70	0.024
55	0.027
40	0.029
35	0.031
30	0.042
18	0.054
12	0.056
9	0.061

L1 and L2 (L1 and L3 have 42% of overlap). Additionally, the L1 and L2 overlap percentage is reduced to 55% by reducing the most outer beam to 49°. Therefore, for this scenario, two overlap percentages of 70% and 55% between L1 and L2 are considered.

- **Scenario b**: The overlap exists between L1 and L2, but L3 drops out. Overlaps of 40% and 35% are obtained by reducing the most outer beam to 40° and 38°, respectively.
- **Scenario c**: The L2 line is excluded, and hence the overlap exists between L1 and L3. Overlap percentages of 30%, 18%, 12% and 9% between L1 and L3 are obtained by reducing the most outer beams to 55°, 51°, 49° and 48°, respectively.

It should be noted that for the calculations presented in Fig. 13, the water depth and the linespacing are both around 25m. Shown in Fig. 14 is the depth standard deviation for the area indicated as 3 in Fig. 5 and 12 after applying the SSP inversion method for the situations with an overlap of 70% (a), scenario a with the maximum swath width, and 30% (b), scenario c derived from excluding every other sailed track while reducing the swath with to 55°. Generally, a reduction in the overlap increases the depth standard deviation. As the overlap decreases, the inversion is carried out

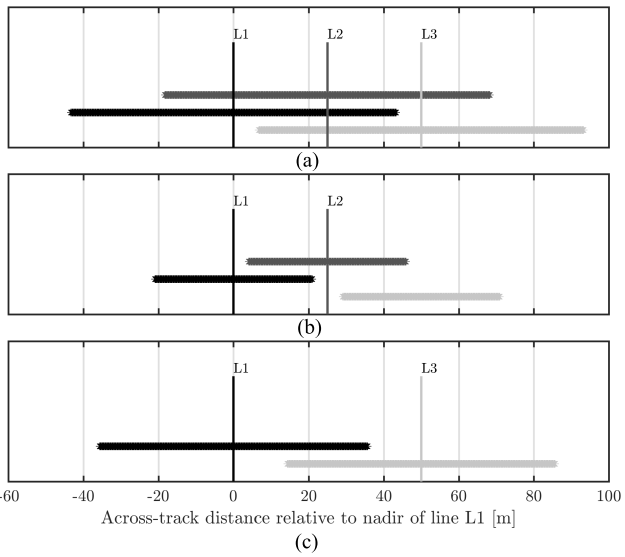

FIGURE 13. Schematic overview of the overlap between the three sailed tracks for 3 scenarios, (a) the overlap exist between L1, L2 and L3 lines, (b) the overlap exist between L1 and L2, (c) L2 is excluded and the overlap exist between L1 and L3. Varying shades of gray show the swath for each sailed track.

where the soundings away from nadir are excluded. The remaining beams are less affected by erroneous sound speeds than the outer beams, and hence not only are there less depth measurements constraining the estimate, but also is the geometry such that the objective function is less sensitive to changes in the unknowns, see [25].

Shown in Table2 is the standard deviation of the difference between the original depths and those derived after applying the inversion method for varying overlap percentages. As expected, a decrease in the overlap percentage increases the standard deviation. For overlap percentages decreasing from 70% to 35%, the standard deviation only

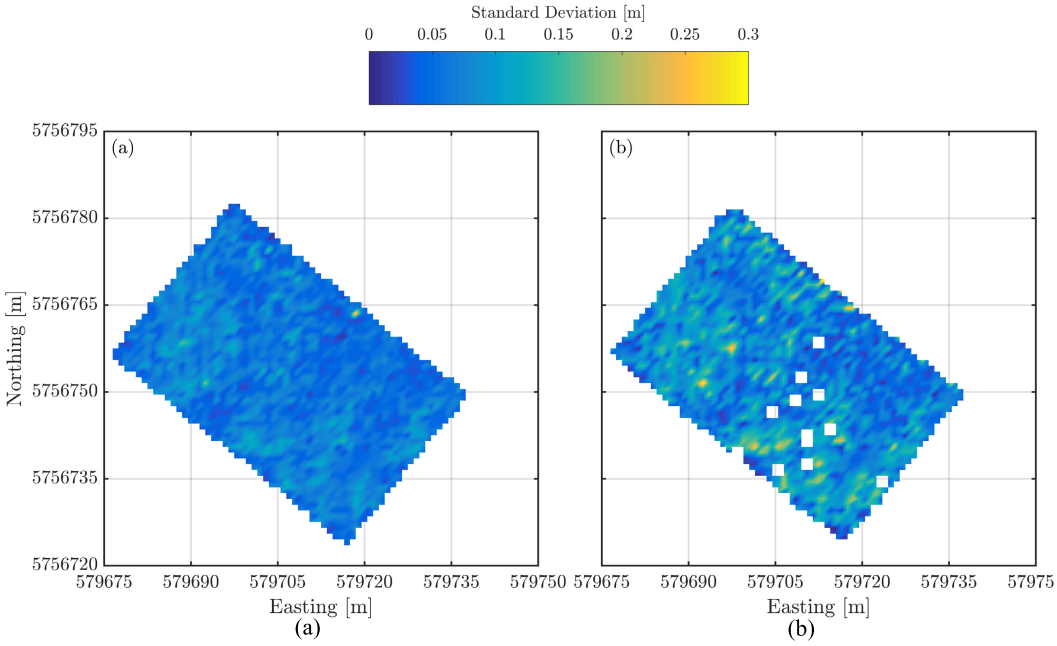

FIGURE 14. Depth standard deviation for area indicated as 3 in Fig. 5 after applying the SSP inversion for a grid with the cell size of 0.25m × 0.25m using (a) 70% overlap and (b) 30% overlap between the adjacent sailing tracks.

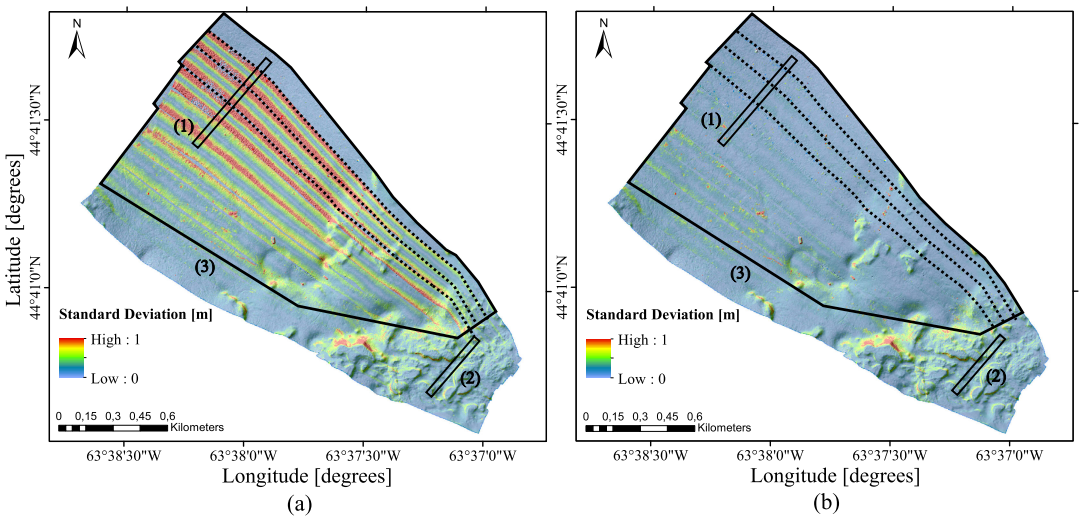

FIGURE 15. Standard deviation of depth measurements in Bedford Basin (a) using the measured SSPs and (b) after applying DE based SSP inversion method. The areas indicated by 1, 2 and 3 are investigated further. The dashed lines indicate 3 sailed tracks.

slightly increases. For an overlap of less than 35%, a more rapid increase is found.

C. ILLUSTRATION OF USE OF THE PROPOSED METHOD IN PRACTICE: APPLICATION TO BEDFORD BASIN

As mentioned in Section III, the bathymetry measurements in the northeast of the Bedford Basin survey area are negatively affected by the unknown sound speed profile. Shown in Fig. 15(a) is the standard deviation of the depth measurements gridded using a cell size of 3m × 3m. The map indicates a larger standard deviation for the outer beams in the northeast of the survey area, see the three sailed tracks shown by dashed lines in Fig. 15 as an example.

Generally speaking, there are a number of error sources with a similar signature as the refraction induced errors. Before applying the proposed inversion method, one should ensure that these contributors have not affected the data set. Besides the uncertainties inherent to the MBES, the contributors affecting the quality of the derived depths can be categorized as static and dynamic. A detailed discussion on the various systematic error sources can be found in [31].

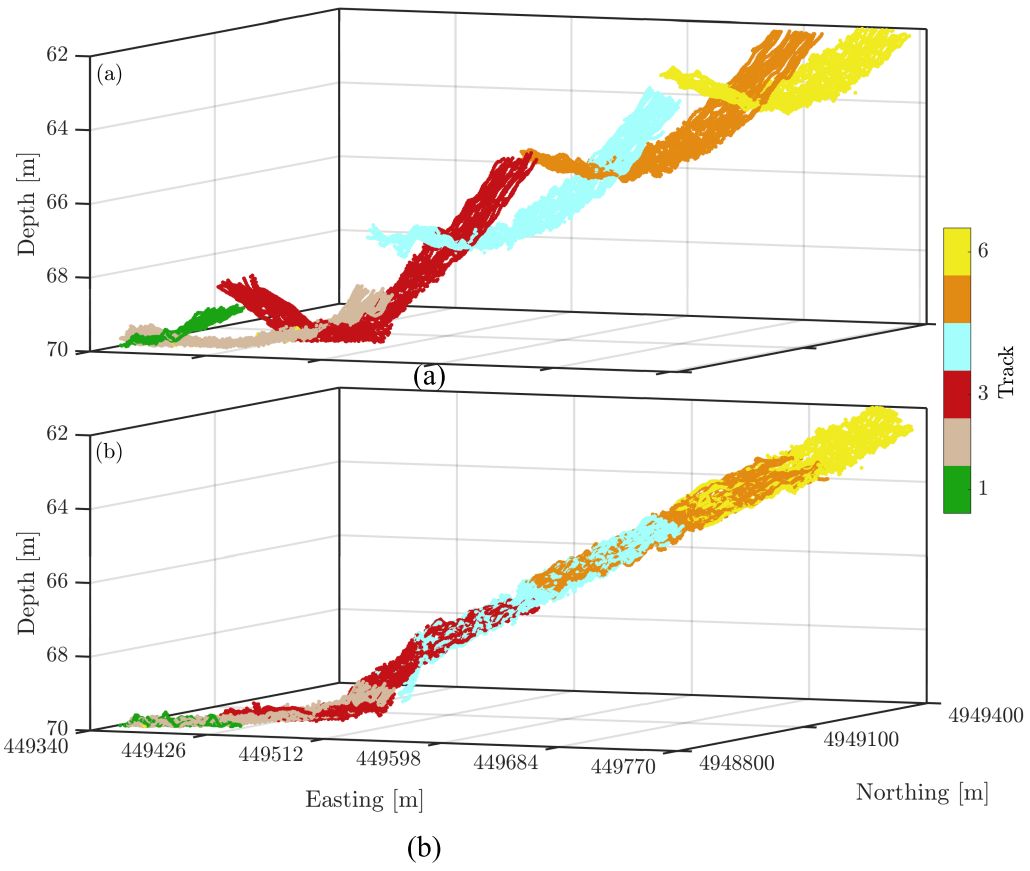

FIGURE 16. Depths within the area consists of 20 pings indicated as 1 in Fig. 15 based on the (a) measured SSPs and (b) result of DE based SSP inversion. Varying colors indicate different sailed tracks.

The static contributor with a similar signature as the refraction is roll misalignment between the MBES and the Inertial Navigation Sensor (INS). The correction of the static systematic errors is mostly done using the patch test, which examines the repeatability of the system over a pre-defined patch of the seafloor. For the Bedford Basin survey, the patch test was carried out, and therefore these systematic errors, if present, have been excluded. The other group of systematic errors are the dynamic ones and produce errors that vary either with periods of the ocean wave spectrum or with long period acceleration of the vessel [8]. The dynamic errors having the same characteristics as the refraction induced error are motion scaling problems (correlating with roll), time delays in the motion sensor output (correlating with roll rate) and imperfect alignment of the roll/pitch axes with the MBES reference frame (correlating with pitch). These errors can be identified using a correlation analysis between the motion time series and depth derivatives. The motion time series have been examined carefully and no signatures of the dynamic systematic errors have been found. Therefore, it is concluded that the observed increase in the differences toward the outer parts of the swath is not caused by systematic error sources.

Applying the DE based SSP inversion algorithm and recalculating the bathymetry using the estimate of the sound speeds correct for the refraction effect, as shown in Fig. 15(b). The method also reduces the standard deviation in other areas where the effect of the unknown/wrong sound speed is less noticeable. It is seen that the bathymetry has been corrected for the vast majority of the data set. The remaining larger uncertainties for the overlapping parts of the swaths can be due to the increasing inherent MBES uncertainties with beam angle. Similar to the previous data set (Nieuwe Waterweg), GN based SSP inversion is also applied and no significant differences were found between the results of applying DE and GN to this data set.

To assess the two surfaces in more detail, two regions of the survey area consisting of approximately 20 pings with and without apparent artefacts have been chosen, see the areas indicated by 1 and 2 in Fig. 8 and 15, respectively. Shown in Fig. 16 are the depths for an area with artefacts, i.e., area 1, before (a) and after (b) the application of the DE inversion method. The DE SSP inversion method clearly corrects the smiley feature presents in the original surface.

Concerning area 2, as seen from the bathymetry map of Fig. 8, morphological features exist to the southeast of the survey area where the depth gets shallower. No refraction problem exists in this area and the variations of the standard deviations are mostly due to the inherent uncertainties

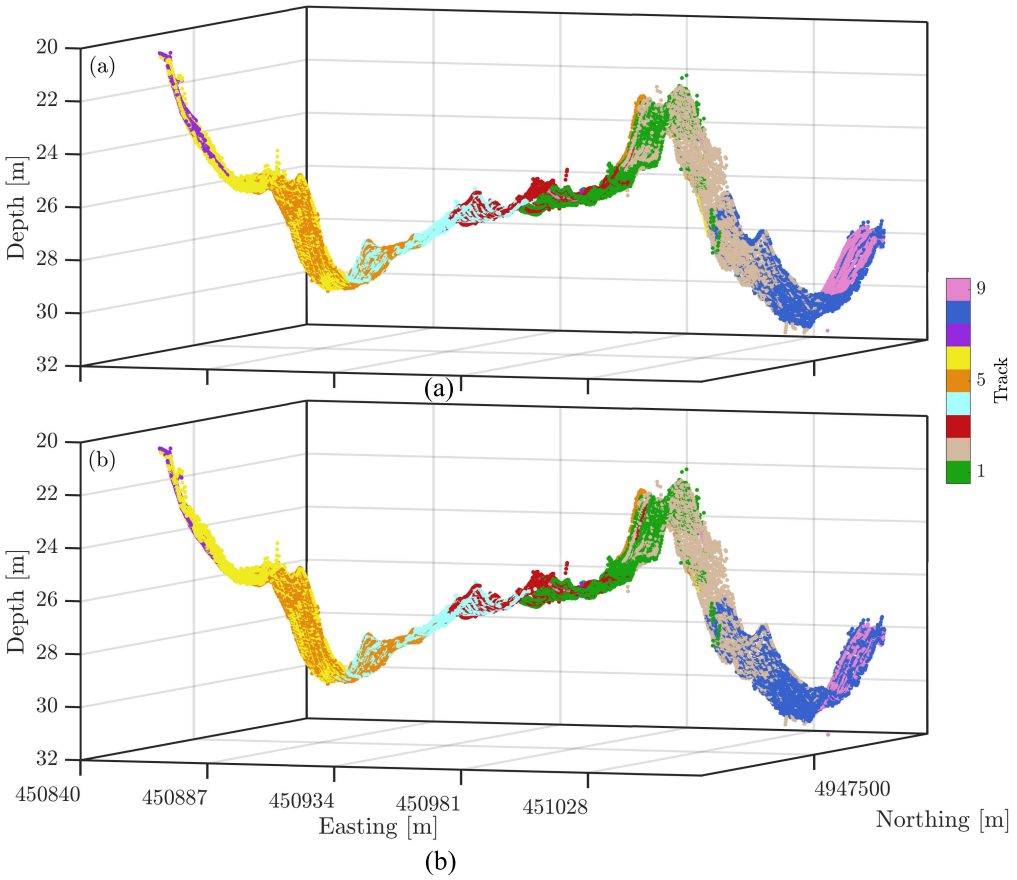

FIGURE 17. Depths within the area consists of 20 pings indicated as 2 in Fig. 15 based on the (a) measured SSPs and (b) result of DE based SSP inversion. Varying colors indicate different sailed tracks.

of the MBES and morphological features. This is thus an interesting area for the assessment of the SSP inversion method accuracy, i.e., to assess whether the application of the method in an area without refraction artefacts introduces neither artificial bathymetric features nor manipulates the existing ones. Fig. 17 illustrates the depths derived before, (a) and after, (b) applying the DE based SSP inversion for the area indicated by 2 in Fig.8, 15. The depths based on the measured SSPs and those optimized are in good agreement. The mean of the differences between the depths using the measured SSPs and those derived after DE based inversion is 0.003m with a standard deviation of 0.078m and based on the Chebyshev's inequality, [26], which is used in case of having an unknown distribution for a random variable, one can state that there is no evidence that the original depth and those after the inversion are different from a statistical point of view.

The histogram of the depth standard deviation for the area indicated as 3 in Fig. 8 and 15 is presented in Fig. 18 using the bathymetry derived from the measured SSPs, (a), and recalculated after applying the DE based SSP inversion, (b). The mean and standard deviation of the depth standard deviation after applying the inversion method decreased by a factor of around 2.75 compared to the situation where the measured SSPs were used. This indicates that the standard deviation not only does get closer to zero but also does vary less from one cell to another.

D. COMPARISON BETWEEN DIFFERENTIAL EVOLUTION AND GAUSS-NEWTON BASED SSP INVERSION METHODS

As discussed, the SSP inversion method can be implemented using either DE or GN based optimization approaches. The former is more powerful as it searches for the global minima as opposed to the latter which can get trapped at a local minimum. As an example, if the starting point is too far from the global optimum, GN is not a suitable approach for localizing it. Moreover, developing the existing model to account for more complicated representations of the SSP in the water column (potentially for the future developments of the SSP inversion method) is more straightforward with DE than GN. This is due to the fact that the former only requires updating the parameter space while the latter needs updating the observation equations and the Jacobian matrix which consist of the partial derivatives of the observation equation with respect to the unknown parameters. However, the GN has the advantage of being faster than DE. The computational complexity of GN is in the order of $O(m^3)$ with m being the number of sound speeds to be optimized plus the number

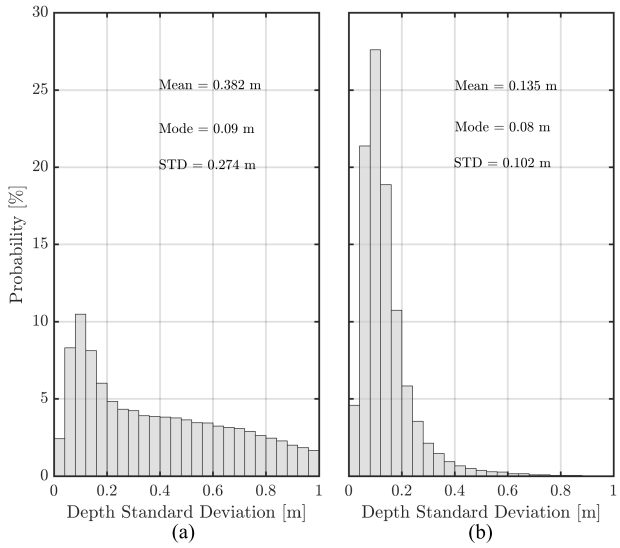

FIGURE 18. Histograms of the standard deviation of the depths derived from (a) measured SSPs and (b) recalculated after applying the DE based SSP inversion.

of cells. Calculating the computational complexity of DE in terms of the big O notation ($O(...)$) is not trivial, because many other parameters such as the population size and multiplication factor can also affect its performance. Therefore, instead of big O notation representation, we have assessed the computational complexity of both methods by comparing the time it takes to run them on the same data sets. The results has indicated that the GN is faster that DE by a factor varying from 3.3 to 5. This observation is a result of both algorithmic complexity and implementation related effects.

V. SUMMARY AND CONCLUSION

In the present contribution, a method for reducing the MBES bathymetric errors induced due to an erroneous/insufficient knowledge of the water column sound speed is presented. The method takes advantage of the overlap between the adjacent sailed tracks and optimizes the sound speeds minimizing the difference between the depth measurements at these overlapping parts. For the optimization, two methods, i.e., DE and GN were used. For the DE, the search was carried out for those sound speed profiles that result in minimum variation of the depth standard deviation along overlapping parts of adjacent swaths. This approach allows for arbitrary parameterizations of the water column SSP. A drawback, however, is the large number of forward calculations required. Alternatively, GN can be used where the optimization is carried out by minimizing the sum of the squares of the difference between modeled and measured OWTT.

A complex environment with varying water column sound speed and free of refraction artefacts was considered and refraction artefacts were introduced assuming erroneous SSPs. Applying the method based on the assumption of constant sound speed to this survey area indicates a good agreement between the original depth measurements and those derived after applying the inversion to the data artificially contaminated by refraction errors. The mean and standard deviation of the differences are 0.009m and 0.024m, respectively. The statistical significance of the differences has been tested using null and alternative hypotheses and it has been shown that the differences between the original and inverted depths are not statistically significant for a 95% confidence interval. This means that even for a situation in which the sound speed varies with depth, the inversion method based on a simple representation of the water column SSP can give reasonable results.

The impact of varying overlap percentages between the adjacent sailed tracks is assessed by considering a small area consisting of 50 pings where the soundings from 4 sailed tracks are located within the area. Various overlap percentages are obtained by reducing the swath width or excluding sailed tracks from the analysis or a combination of both. It is shown that, in general, the reduction of the overlap percentage increases the standard deviation of the difference between the original depths and those derived after applying the inversion method. However, this increase occurs more rapidly for the overlap percentages of less than 35%. For larger values, the reduction of the overlap percentage only slightly increases the standard deviation.

The inversion method was also applied to a data set with existing refraction artefacts at some parts of the surveyed area. Based on the results, applying the method corrects for the apparent refraction artefacts. The method also reduces the standard deviation in other areas where the effect of the unknown/wrong sound speed is less noticeable. For areas without refraction artefacts, the method introduces neither artificial bathymetric features nor manipulates the existing ones. The mean of the differences between the depths before and after applying the inversion method for this area is 0.003m with a standard deviation of 0.078m. Application of Chebyshev's inequality shows that there is no evidence that the original depth and those derived after inversion are different from a statistical point of view. The remaining larger uncertainties for the overlapping parts of the swaths can be due to the increasing inherent MBES uncertainties with beam angles.

For a constant water column sound speed, no significant difference is found between the results of the DE and GN. The latter is however faster by a factor varying from 3.3 to 5 than the former. The advantage of using DE for the optimization lies in its flexibility with regards to SSP parameterizations. If one tends to consider a more complicated representation of the sound speed in the water column, GN becomes inefficient as it involves calculating the derivatives.

APPENDIX A
RECALCULATING LAUNCH ANGLE AND AZIMUTH FOR UPDATES TO SOUNDING ESTIMATES

Consider the situation where both beamsteering is based on the erroneous sound speed (v_m), but that the true sound speed (v) becomes available afterwards. Then the beam vector

has to be re-pointed. Traditionally, re-pointing a beam to account for an update of the sound speed at the transducer is done by correcting the raw steering angles θ reported by the transducer followed by recalculating the beam launch angle, d in Fig. 1, see [23], [24]. However, in this contribution the refraction correction is applied to the launch angle, without having to recalculate θ, leading to an increase in the processing speed.

Before proceeding, it is necessary to introduce the coordinate systems and rotations used. For the vessel coordinate system, we consider a right-handed system with the positive X and Y axes pointing towards the starboard and bow, respectively. Consequently, the Z points towards up. X, Y and Z belong to the vessel and are thus not shown in Fig. 1.

For the navigation frame, shown in Fig. 1 with subscript N, again a right-handed coordinate system considered with the positive X_N, Y_N and Z_N pointing toward east, north and up, respectively.

For rotations, heading (h), pitch (p) and roll (r) are considered to be clockwise or left handed rotations about the Z axis, counter clockwise or right handed rotation about the X axis and counter clockwise rotations about the Y axis, respectively. Tait-Bryant ordering of angle rotation is used, i.e. h,p,r. These rotations are both valid in the vessel and navigation frames.

In general, MBES measurements are stored such that the beam vector (dashed line in Fig. 1) is reported relative to the navigation frame. Therefore, when accounting for an updated sound speed profile, i.e., a modified value for d, requires to translate the beam vector from the navigation frame to the transducer frame. For this, two rotation matrices are needed. One for the vessel motion R_{NV} translating the coordinates from the vessel frame (V) to navigation frame (N) using heading, roll and pitch angles of the vessel relative to the navigation frame measured by the motion sensor. The second rotation required is for the transducer mounting angles (R_{VT}) which translates from the transducer frame (T) to vessel frame (V) using the mounting angles of the MBES receiving array. The rotation matrix from the transducer to the navigation frame is thus derived from the product of these rotation matrices ($R_{NT} = R_{NV}R_{VT}$).

Given the correct launch (d) angle, and the correct azimuth (α), a beam unit vector is defined in the navigation frame ($\vec{u}_N$) which reads as

$$\begin{aligned}\vec{u}_N &= \begin{bmatrix} x_N & y_N & z_N \end{bmatrix}^T \\ &= \begin{bmatrix} \sin\alpha\cos d & \cos\alpha\cos d & -\sin d \end{bmatrix}^T, \end{aligned} \quad \text{(A.1)}$$

where x_N, y_N and z_N are the components of the beam unit vector in the navigation frame. (A.1) can be also written for the erroneous sound speed v_m (inducing errors in the launch angle (d_m) and azimuth (α_m)) and is referred to $\vec{u}_N^m$. The beam unit vector in the navigation frame is then rotated into the transducer frame ($\vec{u}_T$) using $R_{NT}^T\vec{u}_N$. Shown in Fig. 19 are the components of $\vec{u}_T$ in the transducer frame assuming erroneous (a) and correct (b) sound speeds where θ_m and θ

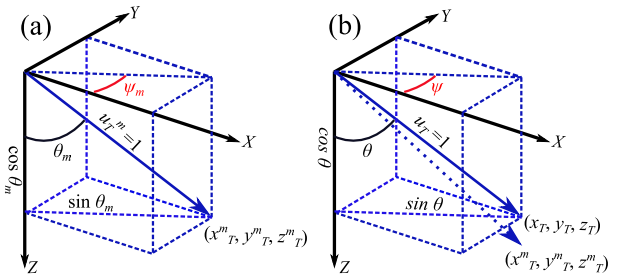

FIGURE 19. Beam vector in transducer frame (*T*) for erroneous (a) and correct (b) sound speeds.

are the erroneous and correct beam vector angles relative to the transducer frame's normal respectively.

Whereas in general d is calculated from θ, here a different approach is taken as described below. Snell's law of refraction for the erroneous and correct beam vectors states

$$\frac{\sin\theta_m}{\sin\theta} = \frac{v_m}{v}. \quad \text{(A.2)}$$

This can be rearranged to describe the angle transformation as

$$\theta = \sin^{-1}\Big(a\sin\theta_m\Big), \quad \text{(A.3)}$$

where $a = \frac{v}{v_m}$ is the ratio of correct to erroneous sound speeds. Considering $\sin\theta$ (or $\sin\theta_m$) as the hypotenuse of the right-angled triangle with the catheti legs x_T (or x_T^m) and y_T (or y_T^m) one can write

$$\begin{aligned}\sin\theta_m &= \sqrt{(x_T^m)^2 + (y_T^m)^2} \\ \sin\theta &= \sqrt{x_T^2 + y_T^2}. \end{aligned} \quad \text{(A.4)}$$

Substituting θ_m and θ from (A.4) in Fig. A.3 gives

$$\begin{aligned}\overbrace{\sin^{-1}\sqrt{x_T^2 + y_T^2}}^{\theta} &= \sin^{-1}\Big(a\sin\overbrace{\Big[\sin^{-1}\sqrt{(x_T^m)^2 + (y_T^m)^2}\Big]}^{\theta_m}\Big) \\ \sqrt{x_T^2 + y_T^2} &= a\sqrt{(x_T^m)^2 + (y_T^m)^2}. \end{aligned} \quad \text{(A.5)}$$

Considering the beam vector in the transducer frame as unitary gives the constraints

$$\begin{aligned} 1 &= u_T^2 = x_T^2 + y_T^2 + z_T^2 \\ 1 &= (u_T^m)^2 = (x_T^m)^2 + (y_T^m)^2 + (z_T^m)^2. \end{aligned} \quad \text{(A.6)}$$

Substituting (A.5) in the expression for u_T^2 in (A.6) gives the third component of the beam vector for the correct sound speed (z_T) as

$$\begin{aligned}|z_T| &= \sqrt{1 - a^2((x_T^m)^2 + (y_T^m)^2)} \\ &= \sqrt{1 - a^2(1 - (z_T^m)^2)}. \end{aligned} \quad \text{(A.7)}$$

As the refraction only changes the beam vector in the plane formed by the Z-axis and the beam vector, the orientation of the projected beam vector onto the XY-plane of the transducer frame remains unchanged for both erroneous and correct

sound speeds ($\psi = \psi_m$ in Fig. 19). This results in the following expressions for x_T and y_T

$$x_T = a x_T^m$$
$$y_T = a x_T^m. \quad \text{(A.8)}$$

(A.7) and (A.8) give the three components of the unit beam vector in the transducer frame for the correct sound speed ($\vec{u}_T$). This vector is then rotated back into the navigation frame using R_{NT} and the correct launch angle and azimuth are derived as

$$d = -\sin^{-1}(z_N)$$
$$\alpha = -\tan^{-1}(\frac{x_N}{y_N}). \quad \text{(A.9)}$$

where x_N, y_N and z_N are the components of the beam unit vector in the navigation frame corresponding to the actual, i.e., correct, sound speed, see (A.1).

ACKNOWLEDGMENT

The SSP inversion method presented in this contribution has been implemented in Qimera post-processing software. The authors would like to thank Quality Positioning Services (QPS) for providing an implementation platform.

REFERENCES

[1] X. Lurton and J.-M. Augustin, "A measurement quality factor for swath bathymetry sounders," *IEEE J. Ocean. Eng.*, vol. 35, no. 4, pp. 852–862, Oct. 2010.

[2] L. Hellequin, J.-M. Boucher, and X. Lurton, "Processing of high-frequency multibeam echo sounder data for seafloor characterization," *IEEE J. Ocean. Eng.*, vol. 28, no. 1, pp. 78–89, Jan. 2003.

[3] A. Furlong, B. Beanlands, and M. Chin-Yee, "Moving vessel profiler (MVP) real time near vertical data profiles at 12 knots," in *Proc. OCEANS MTS/IEEE Conf. Proc.*, Oct. 1997, pp. 229–234.

[4] D. L. Rudnick and J. Klinke, " The underway conductivity–temperature–depth instrument," *J. Atmos. Ocean. Technol.*, vol. 24, no. 11, pp. 1910–1923, Nov. 2007.

[5] D. F. Dinn, B. D. Loncarevic, and G. Costello, "The effect of sound velocity errors on multi-beam sonar depth accuracy," in *Proc. MTS/IEEE. OCEANS Challenges Changing Global Environ.*, vol. 2, Oct. 1995, pp. 1001–1010.

[6] D. S. Cartwright and J. E. H. Clarke, "Multibeam surveys of the Frazer river delta, coping with an extreme refraction environment," in *Proc. Can. Hydrograph. Conf.*, May 2002, pp. 1–23.

[7] W. J. Capell, "Determination of sound velocity profile errors using multi-beam data," in *Proc. Oceans 21st MTS/IEEE Riding Crest Century. Conf. Exhib.*, vol. 3, Sep. 1999, pp. 1144–1148.

[8] J. E. H. Clarke, "Dynamic motion residuals in swath sonar data: Ironing out the creases," *Int. Hydrogr. Rev.*, vol. 4, no. 1, pp. 6–23, Jan. 2003.

[9] J. Beaudoin, B. Calder, J. Hiebert, and G. Imahori, "Estimation of sounding uncertainty from measurements of water mass variability," *Int. Hydrogr. Rev.*, no. 2, pp. 20–38, Nov. 2009.

[10] J. Beaudoin, "Real-time monitoring of uncertainty due to refraction in multibeam echo sounding," *Hydrogr. J.*, vol. 134, pp. 3–13, Feb. 2010.

[11] G. Masetti, J. G. Kelley, P. Johnson, and J. Beaudoin, "A ray-tracing uncertainty estimation tool for ocean mapping," *IEEE Access*, vol. 6, pp. 2136–2144, 2017.

[12] X. Geng and A. Zielinski, "Precise multibeam acoustic bathymetry," *Mar. Geodesy*, vol. 22, no. 3, pp. 157–167, Jul. 1999.

[13] G. Imahori and J. Hiebert, "An algorithm for estimating the sound speed component of total depth uncertainty," in *Proc. Can. Hydrograph. Conf.*, 2008.

[14] L. R. LeBlanc and F. H. Middleton, "An underwater acoustic sound velocity data model," *J. Acoust. Soc. Amer.*, vol. 67, no. 6, pp. 2055–2062, Jun. 1980.

[15] D. B. Cousins and J. H. Miller, "A model based system for simultaneously estimating bathymetry and sound speed characteristics-simulation results," in *Proc. OCEANS MTS/IEEE Conf. Exhibit.*, vol. 1, Sep. 2000, pp. 213–219.

[16] D. B. Cousins and J. H. Miller, "A model based system for simultaneously estimating bathymetry and sound speed profile characteristics-non-isovelocity simulation results," in *Proc. OCEANS MTS/IEEE*, vol. 2, Oct. 2002, pp. 1098–1108.

[17] B. R. Calder, B. J. Kraft, C. de Moustier, J. Lewis, and P. Stein, "Model-based refraction correction in intermediate depth multibeam echosounder survey," in *Proc. 7th Eur. Conf. Underwater Acoust.*, Jul. 2004, pp. 795–800.

[18] E. Kammerer and J. E. H. Clarke, "A new method for the removal of refraction artifacts in multibeam echosounder systems," in *Proc. Can. HydroGraph. Conf.*, Jan. 2000.

[19] J. Ding, X. Zhou, and Q. Tang, "A method for the removal of ray refraction effects in multibeam echo sounder systems," *J. Ocean Univ. China*, vol. 7, no. 2, pp. 233–236, May 2008.

[20] S. Jin, W. Sun, J. Bao, M. Liu, and Y. Cui, "Sound velocity profile (SVP) inversion through correcting the Terrain distortion," *Int. Hydrogr. Rev.*, vol. 13, pp. 7–16, Feb. 2016.

[21] R. Storn and K. Price, "Differential evolution—A simple and efficient heuristic for global optimization over continuous spaces," *J. Global Optim.*, vol. 11, no. 4, pp. 341–359, Dec. 1997.

[22] J. Nocedal and S. J. Wright, *Numerical Optimization*, 2nd ed. New York, NY, USA: Springer, 2006.

[23] J. Beaudoin, J. Hughes Clarke, and J. Bartlett, "Retracing (and re-raytracing) Amundsen's journey through the northwest passage," in *Proc. Can. Hydrograph. Conf.*, Ottawa, ON, Canada, 2004.

[24] J. Beaudoin, J. H. Clarke, and J. Bartlett, "Application of surface sound speed measurements in post-processing for multi-sector multibeam echosounders," *Int. Hydrogr. Rev.*, vol. 5, no. 3, Dec. 2004.

[25] M. Snellen and D. G. Simons, "An assessment of the performance of global optimization methods for geo-acoustic inversion," *J. Comput. Acoust.*, vol. 16, no. 2, pp. 199–223, Jun. 2008.

[26] P. J. G. Teunissen. (2000). *Adjustment Theory: Introduction (Mathematical Geodesy and Positioning)*. VSSD. [Online]. Available: https://www.bookdepository.com/Adjustment-Theory-P-J-G-Teunissen/9789040719745

[27] T. C. Gaida, T. A. T. Ali, M. Snellen, A. Amiri-Simkooei, T. A. G. P. Van Dijk, and D. G. Simons, "A multispectral Bayesian classification method for increased acoustic discrimination of seabed sediments using multi-frequency multibeam backscatter data," *Geosciences*, vol. 8, no. 12, p. 455, Dec. 2018.

[28] D. Buscombe and P. E. Grams, "Probabilistic substrate classification with multispectral acoustic backscatter: A comparison of discriminative and generative models," *Geosciences*, vol. 8, no. 11, p. 395, Oct. 2018.

[29] J. Beaudoin, W. Renoud, T. H. Mohammadloo, and M. Snellen, "Automated correction of refraction residuals," in *Proc. Hydro Conf. Trade Exhibit.*, Nov. 2018, pp. 1–16.

[30] W. K. W. Li and W. G. Harrison, "Propagation of an atmospheric climate signal to phytoplankton in a small marine basin," *Limnol. Oceanogr.*, vol. 53, no. 5, pp. 1734–1745, Sep. 2008.

[31] A. Godin, "The calibration of shallow water multibeam echo-sounding systems," M.S. thesis, Dept. Geodesy Geomatics Eng., Univ. New Brunswick, Fredericton, NB, Canada, 1998. [Online]. Available: http://www2.unb.ca/gge/Pubs/TR190.pdf

TANNAZ H. MOHAMMADLOO was born in Tehran, Iran, in 1987. She received the bachelor's and master's degrees in survey engineering and geodesy from the University of Esfahan, Iran, in 2011 and 2013, respectively. She is currently pursuing the Ph.D. degree with the Acoustics Group, Faculty of Aerospace Engineering, Delft University of Technology (TU Delft), The Netherlands.

Her research interest includes hydrographic operations' improvement.

MIRJAM SNELLEN received the master's degree in aerospace engineering from TU Delft, in 1995, and the Ph.D. degree in geoacoustic inversion from the University of Amsterdam, The Netherlands, in 2002.

She was a Research Scientist with The Netherlands Organization for Applied Research, where she was with Underwater Acoustics Group. She is currently an Associate Professor with the Acoustics Group, Faculty of Aerospace Engineering, Delft University of Technology. Her research interests include the use of acoustic methods for sediment classification, mainly for multibeam (MBES) and single-beam echosounder systems, uncertainty predictions for MBES bathymetric measurements, and marine habitat mapping.

WESTON RENOUD is currently pursuing the M.Sc. degree in geodesy and geomatics engineering with the University of New Brunswick, Canada.

He was a Land Survey Rodman, in 2005. From 2008 to 2011, he was an Acting Hydrographic Chief Survey Technician with science crew aboard, the NOAA Fairweather Ship. He is currently a Senior Hydrographic Software Developer with QPS B.V.

JONATHAN BEAUDOIN received the dual degrees in geomatics engineering and computer science and the Ph.D. degree in marine geomatics from the University of New Brunswick, Canada, in 2001 and 2009, respectively.

From 2010 to 2013, he was a Research Professor with the Center for Coastal and Ocean Mapping, University of New Hampshire, where he researched methods to improve multibeam data acquisition and processing algorithms. He is a Seabed Mapping Specialist over ten years of experience working with multibeam echosounder mapping systems. He is currently the Managing Director, the Chief Scientist, and the Head of Product Management of QPS B.V.

D. G. SIMONS received the M.Sc. degree in physics and the Ph.D. degree from the University of Leiden, Leiden, The Netherlands, in 1983 and 1988, respectively. His Ph.D. research topic involved the development of an imaging gas scintillation spectrometer for X-ray astronomy.

In 1990, he joined the Department of Underwater Technology, The Netherlands Organization for Applied Research Defense, Security and Safety, The Hague, The Netherlands. In October 2006, he was appointed a Fulltime Professor on the Chair Acoustic Remote Sensing, Faculty of Aerospace Engineering, Delft University of Technology. His research interests include multibeam echosounder mapping of seafloor bathymetry, sediment classification through inverse modeling of single- and multibeam echosounder signals, phenomenological approaches to sediment classification, and solving inverse problems in underwater acoustics in general, using global optimization methods, such as genetic algorithms.

Prof. Simons is a member of several committees, including the Scientific Committee of the European Conferences on Underwater Acoustics (ECUA). He is an Associate Editor of the IEEE JOURNAL OF OCEANIC ENGINEERING for the areas bathymetric surveys, mapping, remote sensing, and sonar image processing.